Aerosol and Air Quality Research, 17: 730–740, 2017

ISSN: 1680-8584 print / 2071-1409 online
doi: 10.4209/aaqr.2016.03.0131

The Impacts of Emission Control and Regional Transport on $PM_{2.5}$ Ions and Carbon Components in Nanjing during the 2014 Nanjing Youth Olympic Games

Derong Zhou[1,2], Bing Li[2], Xin Huang[1,3], Aki Virkkula[1,3,4,5], Haisuo Wu[2], Qiuyue Zhao[2], Jie Zhang[2], Qiang Liu[1], Li Li[2], Chunyan Li[2], Feng Chen[2], Siyu Yuan[2], Yuezhen Qiao[2], Guofeng Shen[2], Aijun Ding[1,3*]

[1] *Joint International Research Laboratory of Atmospheric and Earth System Sciences & School of Atmospheric Sciences, Nanjing University, Nanjing 210023, China*
[2] *Jiangsu Key Laboratory of Environmental Engineering, Jiangsu Academy of Environmental Sciences, Nanjing 210036, China*
[3] *Collaborative Innovation Center of Climate Change, Jiangsu Province, China*
[4] *Department of Physics, University of Helsinki, FI-00014 Helsinki, Finland*
[5] *Finnish Meteorological Institute, FI-00560 Helsinki, Finland*

ABSTRACT

Highly time-resolved measurements of water soluble ions, organic and elemental carbon concentrations in the particle diameter size range $D_p < 2.5$ μm ($PM_{2.5}$) were performed at a downwind urban site in Nanjing in the western part of the Yangtze River Delta (YRD) in eastern China during the 2014 Youth Olympic Games (YOG). In this study, we discuss the impacts of emission control in Nanjing and the surrounding areas during the YOG and regional/long-range transport on $PM_{2.5}$ pollution in Nanjing. The average concentrations of NO_3^-, SO_4^{2-}, NH_4^+ were 12.1 ± 9.9, 16.5 ± 9.2, 9.0 ± 5.4 μg m^{-3} during the YOG, and increased 34.3%, 53.7%, 43.9% after the YOG, respectively. The control of construction or on-road soil dust and control of industry led to the decrease of Ca^{2+} concentration by 55% and SO_2 concentration by 46%. However, SO_4^{2-} concentrations remained at relatively high levels, suggesting a significant impact of regional pollution to secondary fine particles in Nanjing. Strong correlations between OC and EC were observed during and after the YOG. A higher percentage (41%) of secondary organic carbon in Nanjing during the YOG periods was consistent with high potential photochemistry and low contributions from coal combustion. Lagrangian dispersion modelling results proved that the city clusters along the Nanjing and Shanghai axis were the major source region for high $PM_{2.5}$ pollution in upwind Nanjing. This work shows that short-term strict control measures could improve the air quality, especially that affected by the primary pollutants; however, regional collaborative control strategy across administrative borders in the YRD is needed for a substantial improvement of air quality.

Keywords: Air quality; Fine particulate matter; Emission control; Regional transport; The 2014 Nanjing Youth Olympic Games.

INTRODUCTION

Intense short-term emission control measures have often been conducted to improve air quality during important events in China, such as the 2008 Beijing Olympic Games, the 2010 Guangzhou Asian Games and the 2010 Shanghai World Expo (Streets *et al.*, 2007; Zhang *et al.*, 2009; Xu *et al.*, 2013; Lin *et al.*, 2013). Assessments of this kind of short-term control measures have provided good opportunities to improve the current understanding of the causes of air pollution and to find a more effective environmental policy for future air pollution control for a specific city or region (Mijling *et al.*, 2009; Wang *et al.*, 2010; Hao *et al.*, 2011; Huang *et al.*, 2013; Liu *et al.*, 2013).

Nanjing, the capital of Jiangsu Province, a highly urbanized and industrialized city located on the western tip of the Yangtze River Delta (YRD) in eastern China (as shown in Fig. 1), hosted the 2nd Youth Olympic Games (YOG) from 16 August to 28 August, 2014. In order to achieve good air quality during this important event, Nanjing and other cities in Jiangsu and the neighbor provinces implemented a series of control measures to reduce emission of air pollutants. The strictest measures were implemented in Nanjing. In this city, one third of the construction facilities had been temporally shut down since 15 July and all outdoor construction works

* Corresponding author.
E-mail address: dingaj@nju.edu.cn

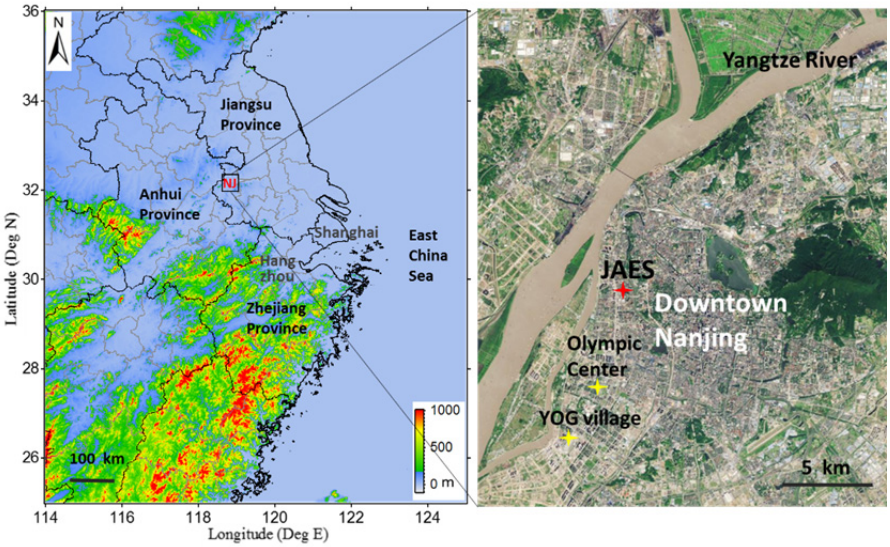

Fig. 1. Map showing cities in the eastern China and location of the JAES site in Nanjing (NJ).

were stopped during 1–26 August. The production of some heavy polluting industries such as the steel, petrochemical, building materials and chemical industries were limited or stopped. Large vehicles with high emissions were forbidden from running in downtown Nanjing. The government put 650 new electric buses and 500 electric taxis into operation and increased the downtown parking fees. The road dust emissions were reduced by using high pressure sprinklers and outdoor barbecue restaurants were banned (Pan *et al.*, 2015; Wang *et al.*, 2015). Because Nanjing is generally downwind of the YRD city clusters, which contribute more than 20% of the national GDP (gross domestic production) in China with only 2% of the land area, and it is under the influence of the prevailing southeast wind in summer (Ding *et al.*, 2013a), additional regional joint control measures were strengthened in 22 cities in the YRD, especially the 8 cities within one hundred kilometers radius to Nanjing. High quality coal was used in the coal-burning units of 162 plants in Jiangsu Province and the power generation fell by 15%, which reduced the sulfur dioxide (SO_2) emissions by more than 20% (Pan *et al.*, 2015). As a result of these efforts, monitoring data from the local environmental protection agency showed quite good air quality during the YOG. However, from the air quality management point of view, it is worthwhile to take this opportunity to make a systematic assessment of the air pollution control during this important event. The assessment is not only important for future air pollution control in Nanjing but also helpful for the whole YRD region.

Either ground-based or satellite measurements can provide good data for the assessment of short-term air quality measures (Mijling *et al.*, 2009; Wang *et al.*, 2010; Ding *et al.*, 2015). However, ground observations with advanced on-line multi-parameter measurements provide sufficient data and more insights into the impact of secondary pollutants (Wang *et al.*, 2010). To assess the impact of air pollution control measures on primary and secondary pollutants during the 2nd YOG, continuous online measurements of ions and carbon components in $PM_{2.5}$ and trace gases were performed at an urban site at JAES (Jiangsu provincial Academy of Environmental Science) in Nanjing during August–September 2014. We mainly used on-line measured secondary inorganic aerosols (SIA = sulfate + nitrate + ammonium) and carbonaceous aerosols composed of black carbon (BC, or elemental carbon, EC) and organic carbon (OC) in this study because recent studies have shown that they are the major secondary components of $PM_{2.5}$ in China (Cao *et al.*, 2007; Shen *et al.*, 2014; Xie *et al.*, 2015). We first investigated the temporal variations of air pollutants before, during and after the YOG, thus estimated the effectiveness of the control measures on the secondary pollutants. The influential processes leading to the formation and accumulation of $PM_{2.5}$ (e.g., sulfate oxidation rate (SOR), nitrate oxidation rate (NOR), and secondary organic carbon (SOC)) are identified. Finally we discussed the characteristics of photochemical aging processes in different air mass and regional transport based on backward trajectory clustering and Lagrangian dispersion modeling.

MEASUREMENT AND METHODOLOGY

Measurement Site

The observing station at Jiangsu provincial Academy of Environmental Science (JAES) is a supersite run by the Jiangsu Key Laboratory of Environmental Engineering. The main purpose of the site is to measure key gaseous and particulate species related to local air pollution and regional transport. The site is located on the rooftop of a 21-floor building (about 80 m above the ground) in the urban area west of Nanjing (118°44′52″E, 32°03′13″N), about 4 km north of the Nanjing Olympic Center and 7 km north of the Youth Olympic Village (shown in Fig. 1). Measurements of aerosols, trace gases and relevant meteorological parameters have been conducted during 8 August–11 September, 2014. All the inlets are approximately 1.5 m above the rooftop of the station. The site is mainly downwind of Nanjing city center since the prevailing winds come from the northeast and

southeast in winter and summer, respectively. Located in the west of the YRD region, the site is also downwind of the most urbanized YRD regions, which is characterized by a cluster of large cities like Shanghai, Suzhou, Wuxi, Changzhou etc. So the measurements at the site can help explore combined impacts of the local and regional air pollutants from these areas of highly intensive human activities.

Instrumentations

The mass concentrations of particles in the diameter ranges $D_p < 2.5$ μm (= $PM_{2.5}$), 2.5 μm < D_p < 10 μm (= PM_{Coarse}) and $D_p < 10$ μm (= PM_{10}) were measured simultaneously with a Thermo Scientific TEOM (Tapered Element Oscillating Microbalance) 1405-DF monitor. The flow rate through sample inlet was 16.67 L min^{-1}, the $PM_{2.5}$ flow rate was 3.0 L min^{-1}, the PM_{Coarse} flow rate was 1.67 L min^{-1}, and the bypass flow was 12 L min^{-1}. The mass concentrations of particles in the diameter ranges Dp < 1 μm (= PM_1) were measured simultaneously with a Thermo Scientific TEOM 1405-F monitor.

For chemical compositions, we only measured water soluble ions and OC/EC of $PM_{2.5}$. Hourly mass concentrations of inorganic ions (SO_4^{2-}, NO_3^-, Cl^-, NH_4^+, Na^+, K^+, Ca^{2+}, Mg^+) and trace gases (NH_3, SO_2, HNO_2, HNO_3, and HCl) were analyzed by a commercially available online analyzer for Monitoring of AeRosols and GAses (MARGA, model ADI 2080, Applikon Analytical B. V. Corp., Netherlands) with a $PM_{2.5}$ sharp-cut cyclone (Ding *et al.*, 2013b; Kong *et al.*, 2014; Xie *et al.*, 2015; Wang *et al.*, 2016). The instrument is comprised of a sampling system and an analytical system. The sampling system consists of one wet rotating denuder (WRD) for gas sampling and one steam jet aerosol collector (SJAC) for aerosol collecting. At a flow rate of 1 $m^3 hr^{-1}$ ambient air was drawn into the sampling box, then after a series of processing two collected liquid samples were analyzed by ion chromatography. A MARGA has been well applied at the SORPES station in Nanjing (Ding *et al.*, 2013b; Xie *et al.*, 2015; Ding *et al*., 2016a).

A semi-continuous OC/EC carbon aerosol analyzer, Sunset Laboratory Inc., was applied to sample ambient air through a $PM_{2.5}$ sharp cut cyclone. The sample air flow onto a pair of quartz fiber membrane filters stacked back to back with a surface area of approximately 1.5 cm^2, located inside a quartz glass oven chamber. The detection limit of the hourly EC and OC data was approximately 0.40 μg m^{-3}. Further details on this instrument are provided elsewhere (Bauer *et al.*, 2009; Wang *et al.*, 2011). The hourly-averaged PM concentrations were used in this work. Meteorological data used in the study were obtained from the local meteorological site with one kilometer distance. The trace gases of SO_2 and NO_2 for the averaged nine state control monitoring stations set by Jiangsu Environmental Monitoring Center were obtained from the pubic platform (http://218.94.78.75/jsair/).

Lagrangian Dispersion Modeling and Backward Trajectory Calculation

To gain insights into the transport characteristics of air pollutants, Lagrangian particle dispersion modeling (LPDM) simulations of the 'footprint' residence time (i.e., retroplumes) were carried out (Ding *et al.*, 2013c). LPDM were calculated by using the Hybrid Single-Particle Lagrangian Integrated Trajectory (HYSPLIT) model, developed in the Air Resource Laboratory (ARL) of the USA National Oceanic and Atmospheric Administration (NOAA) (Draxler and Hess, 1998; Stein *et al.*, 2015). For each hour during the YOG period, 3000 particles were released at 100 m altitude over the site and were traced backward for a 3-day period (Ding *et al.*, 2013a, c). Also 72-h backward trajectories were calculated to identify the origin and transport pathway of large-scale air masses. Both LPDM run and trajectories calculation were driven with GDAS (Global Data Assimilation System) data (http://ready.arl.noaa.gov/HYSPLIT.php), with the endpoint at the JAES, and at an altitude of 100 m above ground level.

RESULTS AND DISCUSSIONS

Chemical Compositions Measured during the YOG

To examine secondary inorganic aerosols pollution during the YOG, the observation at the JAES site from 8 August to 11 September was divided into three periods: 8–15 August, the pre-control period before the YOG (Period 1–P1); 16 August–3 September, the period during and one-week after the YOG with strict control plus emergency control for days with worse meteorological conditions (Period 2–P2); and 4–11 September, the period without any specific control measures (Period 3–P3).

The time series of the concentrations of NO_3^-, SO_4^{2-}, NH_4^+, PM_1, $PM_{2.5}$, and PM_{10} with relative humidity, air temperature, wind speed and direction are shown in Fig. 2. Three pollution episodes were observed in 15–16, 20–23 and 26–28 August during the YOG period. The maximum concentration of the hourly $PM_{2.5}$ was 155.3 μg m^{-3} in the morning of 26 August. According to the time series, the three pollution episodes had some similar characteristics. For example, the increase of PM concentrations started with the enhancement of relative humidity and weakening of wind speed, and the pollution episode weakened accompanied with a relative humidity decrease and wind speed enhancement.

The concentrations of PM and related trace gases in the three periods are compared in Table 1. The average concentrations of $PM_{2.5}$ were 62.0 ± 34.5 μg m^{-3}, 55.1 ± 27.3 μg m^{-3}, and 82.4 ± 22.5 μg m^{-3} in P1-P3, respectively. In contrast to the PM in P1, the averaged levels of PM_1, $PM_{2.5}$ and PM_{10} decreased 5.9%, 11.1% and 6.7% in P2, and increased 48.2%, 32.9% and 39.6% in P3, respectively. Compared with the concentrations in P1, the concentrations of NO_3^-, SO_4^{2-} and NH_4^+ of $PM_{2.5}$ in P2 remained the same level, but increased 34.3%, 53.7%, 43.9% in P3, respectively. In P1 and P2 when the strict control measures came into effect, the concentration levels of PM and SIA were relatively low. The averaged levels of Ca^{2+} observed in P3 were about 2.2-fold that seen during P2 due to closing all the construction facilities in Nanjing during the YOG. The ratio of NO_3^- to SO_4^{2-} ranged from 0.12 to 2.01 during the YOG, with means of 0.74 ± 0.42 and 0.72 ± 0.37 μg m^{-3} in P2 and P3. Cation and anion equivalent concentration (μmol m^{-3}) were calculated using the following equations:

$$\mathrm{CE(cation\ equivalent)} = \frac{Na^+}{23} + \frac{NH_4^+}{18} + \frac{K^+}{39} + \frac{Mg^{2+}}{12} + \frac{Ca^{2+}}{20} \quad (1)$$

$$\mathrm{AE\ (anion\ equivalent)} = \frac{SO_4^{2-}}{48} + \frac{NO_3^-}{62} + \frac{Cl^-}{35.5} \quad (2)$$

The averaged cation-to-anion ratios were 0.95 ± 0.09, 0.98 ± 0.08 and 1.02 ± 0.03 in the three periods, respectively. The reduced alkalinity of the ionic composition during P1 and P2 could be explained as the decrease of fugitive soil dust emission due to the closing of construction and constantly road sprinkler.

The strict emission control measures had little effect on the concentrations of NH_3 since ammonia emissions are mainly from agricultural production and limited traffic control was carried out in Nanjing. However the variations of SO_2 and NO_2 were strongly related to the emission control measures.

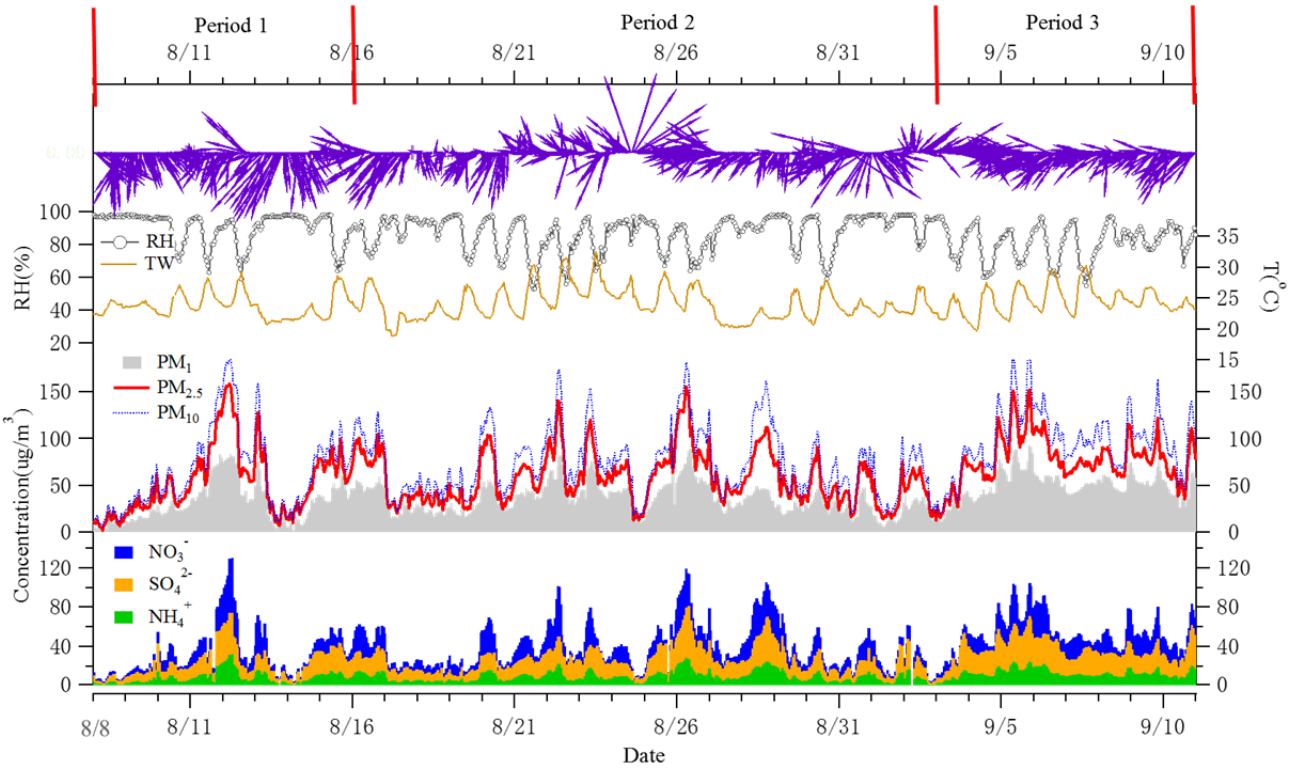

Fig. 2. Time series of NO_3^-, SO_4^{2-}, NH_4^+, PM_1, $PM_{2.5}$, PM_{10} with relative humidity (RH), air temperature (T), wind speed and direction at JAES during the study period. Note: Period 1- The pre-emission control period with limited reduction conducted. Period 2- The period of strict emission control. Period 3- The period without specific emission reduction.

Table 1. Mean concentrations and standard deviations (Mean ± SD) of fine particle NO_3^-, SO_4^{2-}, NH_4^+ and Ca^{2+}, PM_1, $PM_{2.5}$, PM_{10}, SO_2, NO_2, ratio of NO_3^-/SO_4^{2-}, CE/AE with meteorological parameters during three periods in Nanjing.

Mean ± SD (μg m^{-3})	P1	P2	P3
PM_1	35.5 ± 20.7	33.4 ± 15.4	52.6 ± 13.1
$PM_{2.5}$	62.0 ± 34.5	55.1 ± 27.3	82.4 ± 22.5
PM_{10}	75.0 ± 41.3	70.2 ± 34.1	104.7 ± 28.8
NO_3^-	12.79 ± 10.87	12.12 ± 9.9	17.18 ± 9.01
SO_4^{2-}	16.34 ± 8.48	16.54 ± 9.17	25.12 ± 7.31
NH_4^+	9.34 ± 5.90	9.02 ± 5.36	13.44 ± 3.99
Ca^{2+}	0.20 ± 0.19	0.45 ± 0.32	1.00 ± 0.44
NO_3^-/SO_4^{2-}	0.75 ± 0.44	0.74 ± 0.42	0.72 ± 0.37
CE/AE	0.95 ± 0.09	0.98 ± 0.08	1.02 ± 0.03
NH_3	7.6 ± 2.7	6.6 ± 2.3	6.9 ± 2.0
NO_2	30.1 ± 12.0	31.6 ± 13.6	41.7 ± 17.0
SO_2	9.7 ± 6.1	9.8 ± 6.2	18.1 ± 6.9
T (°C)	24 ± 2.1	23.9 ± 2.6	24.7 ± 2.2
RH (%)	88.9 ± 9.9	87.1 ± 10.8	81.0 ± 10.6

The average concentrations of SO_2 and NO_2 were 9.7 ± 6.1 and 30.1 ± 12.0 μg m^{-3} in P1, and 9.8 ± 6.2 and 31.6 ± 13.6 μg m^{-3} in P2, respectively, significantly lower than the respective concentrations of 18.1 ± 6.9 and 41.7 ± 17.0 μg m^{-3} in P3. Control measures such as limiting of heavy pollution industry and using of high quality coal lead to the tremendous decrease of SO_2 in the ambient air in Nanjing. The averaged concentrations of NO_2 were about 3-fold of SO_2, suggesting that NO_2 emission from cars had contributed a lot since no restrictions on public travelling during the YOG. Tu *et al.* (2007) found that the largest fraction of air pollution by NO_x and SO_2 can be attributed to local sources in Nanjing. A recent study showed that the monthly OMI satellite observations showed a 32% decrease of the NO_2 column concentration during the YOG period in Nanjing (Ding *et al.*, 2015). Previous studies also suggested that ambient concentrations of vehicle-related nitrogen oxides dropped by 25% in the first two weeks after full control was put in place in Beijing (Wang *et al.*, 2010), and significant decreases of NO_2 (by 20 %) occurred during the expo in Shanghai (Hao *et al.*, 2011). These results indicated that strong regional emission control significantly improved the short-term air quality, especially for the primary pollutants or short life-time secondary pollutants.

Diurnal Variations

The diurnal variations of Ca^{2+}, $PM_{2.5}$, NH_3, NO_3^-, SO_4^{2-} and NH_4^+ in the three periods are shown in Fig. 3. The early morning (08:00 local time) peaks suggest a great contribution of $PM_{2.5}$ from traffic exhaust, followed with a $PM_{2.5}$ concentration decreased significantly until the afternoon due to the development of the planetary boundary layer. In addition, it is worthwhile to be noticed that the highest peak values occurred in night time (20:00–02:00) during P3, which are about 141–200% of that during the YOG periods.

Different from $PM_{2.5}$ and other water soluble ions including NH_4^+, NH_3 showed similar concentration levels and diurnal patterns in the three periods with low morning peaks and afternoon valleys. NH_3 is mainly emitted from livestock excreta and fertilizer application (Huang *et al.*, 2012) and is difficult to be reduced. There were no special control measures on the emission source of NH_3. Considering the fact that we conducted measurements only for a short period, here the similar diurnal pattern of NH_3 during the three periods reveals that the influence of different meteorological conditions to overall air pollution during different periods is ignorable, and that we can believe the emission control worked in the P1 and P2, compared with P3.

NO_3^- and NH_4^+ showed same concentration levels and patterns as $PM_{2.5}$ in P1 and P2, as well as the nocturnal peaks in P3. There are almost no diurnal variations of Ca^{2+} and SO_4^{2-} in P1 and P2 due to the strong emission control. However, obvious diurnal variation and higher concentration levels of Ca^{2+} and SO_4^{2-} are observed after the YOG, which clearly demonstrate the effectiveness of control measures taken in P1 and P2. High peak values of Ca^{2+} and SO_4^{2-} were observed in nocturnal (20:00–02:00) in P3, which are about 217–366% and 138–184% higher than in P2, indicating more intensive construction activities accompanied with nocturnal trucks transport after a break more than one month. In addition, the heavy industry eager to boost capacity and burn more coal after the YOG, which also further enhanced the nocturnal pollution. All these factors led to the higher nocturnal secondary inorganic ions in $PM_{2.5}$.

Formation of Secondary Inorganic Aerosols

The conversion of SO_2 to particulate sulfate is mainly via atmospheric reactions both in gas and aqueous phases (Huang *et al.* 2014; Huang *et al.*, 2015). Nitrate is usually generated by oxidation of nitrogen oxides and its following reactions with ammonia through complicated homogeneous and heterogeneous reactions (Utsunomiya and Wakamatsu, 1996). In order to understand the influence of emission control on secondary aerosols formation, we investigated the relationship of sulfate and nitrate with their precursors, i.e., SO_2 and NO_x.

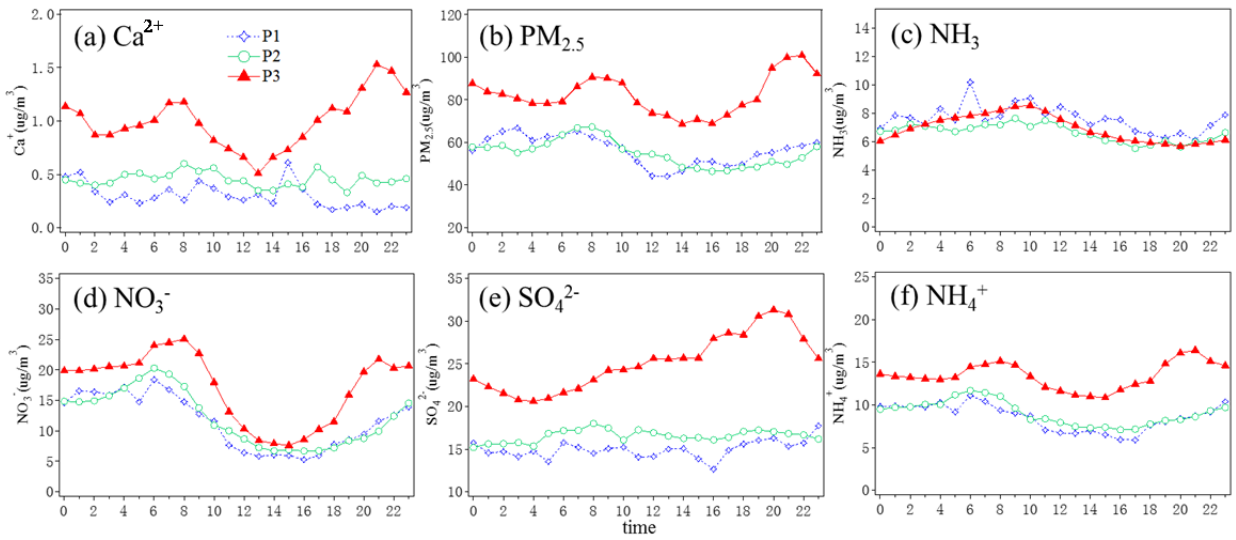

Fig. 3. Averaged diurnal variations of (a) Ca^{2+}, (b) $PM_{2.5}$, (c) NH_3, (d) NO_3^-, (e) SO_4^{2-} and (f) NH_4^+ in the three periods.

Figs. 4(a) and 4(b) give the diurnal variations of SO_4^{2-}/NO_3^- and SO_2/NO_2 in the three periods, respectively. The ratio of SO_2/NO_2 showed an overall broad peak from morning to early afternoon. This pattern could be explained by different emission sources for the two species: NO_2 is mainly from various combustion sources while SO_2 was more from elevated emission sources, such as chimneys of power plants and industries. The development of boundary layer in the morning favored the downwash of nighttime-emitted plumes from residual layer and contributed to the daytime peak (Ding *et al.*, 2013a). However, the SO_4^{2-}/NO_3^- ratio showed a distinguished peak in the later afternoon, which is a combined result from a daytime buildup of sulfate due to secondary formation and a value of NO_3^- due to thermal decomposition in the afternoon (Oxley *et al.*, 1989). It can be seen from Figs. 4(a) and 4(b) that the both ratios showed a similar diurnal pattern for the three periods but much higher SO_2/NO_2 ratio existed in the Period 3, especially in the morning when SO_4^{2-}/NO_3^- ratios were well-matched. This result indicates that the primary pollutants, especially SO_2, were substantially reduced because of emission control, and that observed SO_4^{2-} and NO_3^- aerosols were more from secondary formation of regional sources other than primary emission.

To further exam the secondary formation of sulfate and nitrate, we calculated the oxidation rate for sulfate (SOR) and nitrogen (NOR), respectively, using the following equation:

$$SOR = \frac{nss - SO_4^{2-}}{nss - SO_4^{2-} + SO_2} \quad (3)$$

$$NOR = \frac{nss - NO_3^-}{nss - NO_3^- + NO_2} \quad (4)$$

The nss-SO_4^{2-} and nss-NO_3^- stand for non-sea-salt molar value of SO_4^{2-} and NO_3^-, respectively. The units for SO_2, NO_2, nss-SO_4^{2-} and nss-NO_3^- are moles. Figs. 4(c) and 4(d) give the diurnal cycles of the two ratios during the three periods. The value of SOR varied from 0.15 to 0.82, with a mean of 0.52; and the values of NOR, varied from 0.02 to 0.62 with a mean of 0.21. These values are quite high compared with results obtained at other cities using the same calculation method. For example, Zhou *et al.* (2012) reported the seasonal means for NOR in Beijing were 0.17, 0.15, 0.14, and 0.1 in summer, autumn, spring, and winter, respectively. Tan *et al.* (2009) indicated that average NOR value was much higher in haze days (0.24) than normal days (0.09), and average SOR in haze days (0.29) was slightly higher than that in normal days (0.22) in Guangzhou. The relatively high NOR and SOR in Nanjing suggests vigorous photochemistry and oxidation of precursors due to high atmospheric oxidizing capacity in a humid environment (Xie *et al.*, 2015). Fig. 4(c) showed that NOR was quite similar during the three periods but the SOR in the P3 was completely different from other two periods. It showed a relative lower SOR during night and the early morning but a sharp increase before noontime followed with a board afternoon peak, suggesting a strong daytime secondary production.

Characteristics of Carbonaceous Species

The hourly concentration of EC varied from 0.5 to 6.5 μg m^{-3} during P2 and P3 with an average of 2.6 μg m^{-3}. OC levels increased from the minimum of 2.5 μg m^{-3} to the maximum of 14.0 μg m^{-3} with an average of 6.6 μg m^{-3}. The average OC/EC ratios ranged from 1.03 to 8.67 with an average of 2.78. The results are consistent with the previous studies in Nanjing (Li *et al.*, 2015). EC is essentially a primary pollutant of incomplete combustion from residential

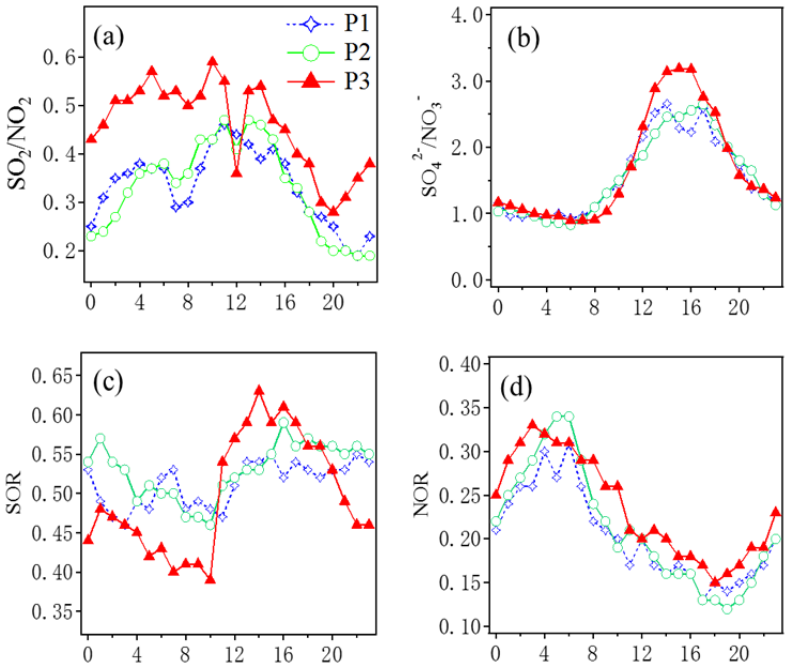

Fig. 4. Average diurnal variation of (a) SO_2/NO_2, (b) SO_4^{2-}/NO_3^-, (c) SOR and (d) NOR in the three periods.

coal, motor vehicle fuel, and biomass (Andersson *et al.*, 2015). OC originates from primary anthropogenic sources like the above-mentioned combustion and also from secondary transformation from gaseous precursors (Cao *et al.*, 2007; Wang *et al.*, 2012). The OC/EC ratio as a function of EC for P2 and P3 was presented in Fig. 5(a). It shows that high OC/EC ratios (> 4.0) were clustered at low EC concentrations (< 2 μg m^{-3}). High temperature (25–33°C) lead to relatively high OC/EC ratios at high EC concentrations (> 2 μg m^{-3}), which suggested a significant effect of the formation of secondary organic carbon (Cao *et al.*, 2007; Wang *et al.*, 2012). Fig. 5(b) showed the correlations between OC and EC in P2 and P3. Strong correlations between OC and EC were observed during the YOG ($r = 0.82$, $p < 0.01$), and after the YOG ($r = 0.61$, $p < 0.01$). It suggests a possible origin from common sources, e.g., the combustion of fossil fuel and motor vehicle emissions. The lower correlation coefficient after the YOG indicated some additional sources of OC existed after the strict emission control measures canceled.

To evaluate the contributions of both primary and secondary organic carbon to carbonaceous aerosol, the equations below are used (Turpin and Huntzicker, 1995):

$$OC_{sec} = OC_{tot} - EC\ (OC/EC)_{min} \quad (5)$$

$$OC_{pri} = EC\ (OC/EC)_{min} \quad (6)$$

where OC_{sec} is secondary OC, OC_{tot} is total OC, OC_{pri} is primary OC, and $(OC/EC)_{min}$ is the minimum ratio of OC/EC, which could replace the ratio of OC to EC in the primary aerosol. The $(OC/EC)_{min}$ in the lowest 15% OC/EC ratios (1.24) would be a reasonable estimate of the primary emissions in this study, which is close to the summer ratio reported in other studies (Yuan *et al.*, 2006; Cao *et al.*, 2007). The fraction of SOC in total carbon (TC) was shown in Fig. 6. SOC accounted for 41% during P2, and 29% of TC during P3, respectively. The higher percentage (41%) of SOC in Nanjing during the YOG periods was consistent with a high potential photochemistry and low contributions from primary coal combustion due to the strict emission control measures.

Regional Transport and its Implications for Air Pollution Control Measures

Meteorological conditions play important roles in air quality through local air pollution accumulation and long-range transport (Ding *et al.*, 2016b; Zhang *et al.*, 2016). The YRD region is located to the south of the most polluted East China, and under the control of the East Asian Monsoon (Zhou *et al.*, 2013). Long-range and regional transport of the air pollutants have been found to be important factors influencing air quality in this region (Ding *et al.*, 2013a; Lin *et al.*, 2013; Shen *et al.*, 2014; Ding *et al.*, 2016a). It is of great importance to investigate the origin and transport pathways of large-scale air masses and chemical composition change in different air masses. Fig. 7 illustrates the five typical pathways of air parcels arriving at Nanjing during the YOG periods. According to the trajectory cluster analysis,

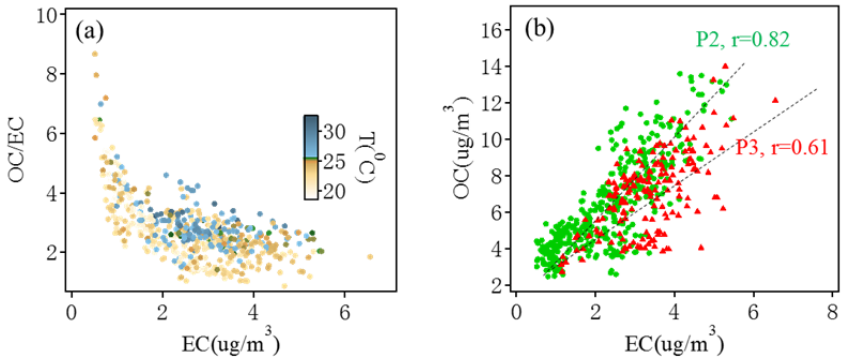

Fig. 5. Scattering plot of (a) OC/EC ratios versus EC concentrations during P2 & P3 and (b) OC concentrations versus EC concentrations in P2 and P3.

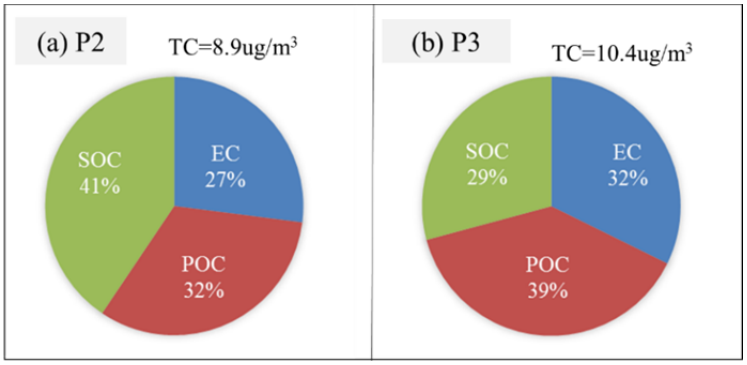

Fig. 6. Relative percentage of primary and secondary sources contributed to total carbon in (a) Period 2, (b) Period 3.

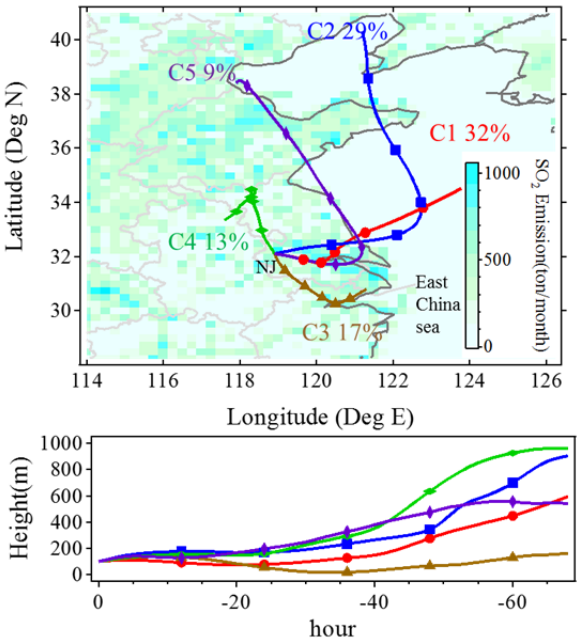

Fig. 7. Averaged 5 typical backward air mass trajectories arrived at Nanjing (NJ) during the YOG period in this study.

72-hr backward trajectories originated from the eastern YRD (C1, 32%), the Yellow Sea and the Bohai Sea (C2, 29%), the Southeastern YRD (C3, 17%), Northwestern YRD (C4, 13%) and eastern coastal area (C5, 9%), respectively. The city clusters in the eastern YRD region showed great contribution of the air masses recorded at Nanjing.

The hourly-averaged mass concentrations of $PM_{2.5}$ and ion and carbon components in the five clusters were show in Table 2. The concentration of $PM_{2.5}$ with air from C1, C2, C3, C4 and C5 were 63.7 ± 24.2, 44.7 ± 16.7, 71.2 ± 25.9, 58.8 ± 30.6, and 105.8 ± 22.9 μg m^{-3}, respectively. The polluted clusters were mainly continental air masses from the eastern coastal area and the Southeastern YRD, while the air masses from marine area and Northwestern YRD were much cleaner. OC in these five clusters were 7.4 ± 1.9, 5.3 ± 1.8, 9.0 ± 2.5, 5.8 ± 2.7, and 8.9 ± 1.0 μg m^{-3}, EC were 2.6 ± 0.9, 1.8 ± 0.9, 3.3 ± 1.0, 2.5 ± 1.1, and 3.4 ± 0.5 μg m^{-3}, respectively. With over 72 hours staying along the city clusters in the eastern China, the air masses came from the eastern coastal area and the southeastern YRD experienced a high photochemical reaction process. So the OC and SOC concentrations in C3 and C5 were highest, indicating high secondary pollutants transported to Nanjing from a regional scale. NO_3^- and SO_4^{2-} in C5 were about two folds of those in other air masses. High emissions of SO_2 and NO_2 in YRD regions combined with a stable continental air mass control could cause high levels of secondary inorganic aerosols in Western YRD via long-range transport. Generally, the pollution sort of air mass travelled to Nanjing ranged from C5, C3, C1, C4 and C2 during the YOG periods. These results suggest an important role of regional transport, especially from the area in eastern coastal China, which was the main potential source region.

To gain a more detailed picture of potential source region of the air masses, averaged retroplumes representing transport pathways of air masses observed at Nanjing were calculated. Fig. 8 shows the different distribution of "footprints" residence time and $PM_{2.5}$ potential source contribution (PSC) with $PM_{2.5}$ concentration greater than 80 μg m^{-3} and less than 40 μg m^{-3}. It can be seen that for the higher pollution episode the air masses recorded at Nanjing mainly came from the eastern China and covered the most polluted YRD cities in the east and southeast, while the clean air masses mainly originated from the East China Sea and Anhui province. These distributions clearly proved that the city clusters along the Nanjing and Shanghai axis were the major source region for high $PM_{2.5}$ pollution in upwind Nanjing, which is consistent with Ding *et al.* (2013a). It should be noted that the $PM_{2.5}$ potential source distribution not only gives a distribution pattern and pathway of air mass, but also directly reveal the locations of emission sources. The strong emission control measures had played key role in improving the air quality during the YOG, but the joint control of the regional emission in YRD may not be as efficient as the 2008 Beijing Olympics (Zhang *et al.*, 2009; Wang *et al.*, 2010; Xing *et al.*, 2011). The results above are indicative of the predominance of secondary transformation via regional transport from YRD and north Shandong Province. The emission of air pollutants in the YRD region has exceeded the environmental capacity, and long-term regional collaborative prevention and control measurements are needed in the future.

CONCLUSIONS

We conducted continuous measurements of chemical components in $PM_{2.5}$ and related trace gases before, during, and after the 2014 Nanjing Youth Olympic Games. Secondary inorganic aerosols, carbonaceous aerosols, trace gases and major meteorological factors were analyzed.

Table 2. Mean concentration and standard deviation (Mean ± SD) of $PM_{2.5}$, OC, EC, SOC, NO_3^-, SO_4^{2-}, NO_3^-/SO_4^{2-}, and NH_4^+ in five different air masses during the YOG period in Nanjing.

Mean ± SD (μg m^{-3})	C1 (32%)	C2 (29%)	C3 (17%)	C4 (13%)	C5 (9%)
$PM_{2.5}$	63.7 ± 24.2	44.7 ± 16.7	71.2 ± 25.9	58.8 ± 30.6	105.8 ± 22.9
OC	7.4 ± 1.9	5.3 ± 1.8	9.0 ± 2.5	5.8 ± 2.7	8.9 ± 1.0
EC	2.6 ± 0.9	1.8 ± 0.9	3.3 ± 1.0	2.5 ± 1.1	3.4 ± 0.5
SOC	4.3 ± 1.4	3.1 ± 1.1	5.0 ± 1.6	2.9 ± 1.7	5.1 ± 1.0
NO_3^-	14.7 ± 9.2	10.4 ± 8.3	14.1 ± 12.7	10.8 ± 10.1	27.1 ± 9.2
SO_4^{2-}	16 ± 4.7	13.4 ± 5.6	19.6 ± 4.9	18.2 ± 10	38.3 ± 7.5
NO_3^-/SO_4^{2-}	0.90 ± 0.51	0.75 ± 0.39	0.71 ± 0.53	0.53 ± 0.28	0.71 ± 0.24
NH_4^+	9.7 ± 3.8	7.2 ± 3.6	9.9 ± 4.4	9.7 ± 6.0	20.3 ± 5.0

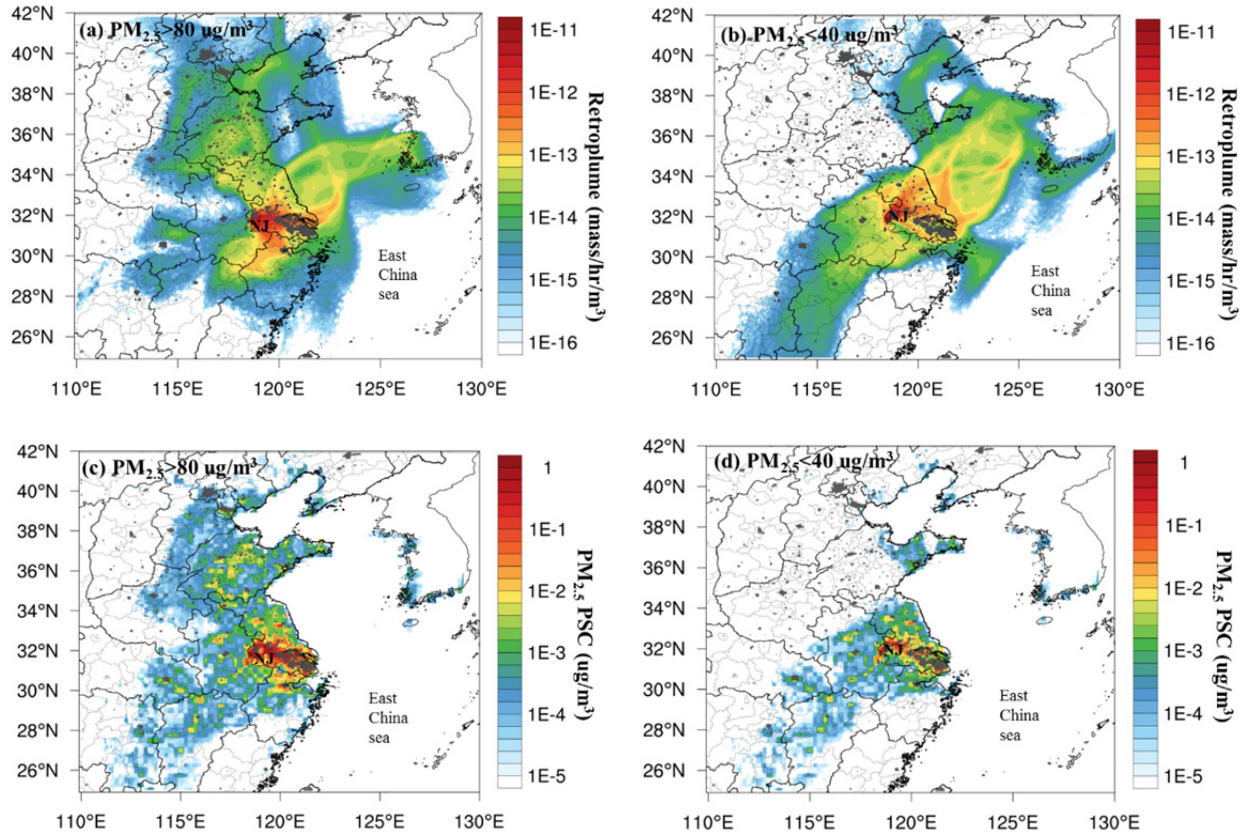

Fig. 8. Averaged retroplume ("footprint" residence time at 100 m altitude) showing (a) transport pathways of air masses and (c) $PM_{2.5}$ PSC at Nanjing (NJ) with $PM_{2.5}$ > 80 μg m^{-3}; (b) averaged retroplume and (d) $PM_{2.5}$ PSC at Nanjing with $PM_{2.5}$ < 40 μg m^{-3} during YOG periods. Grey spots were the distribution of city lights.

The results indicated that air quality in Nanjing was strongly linked both to the control measures and to the regional transport during the YOG. The average concentrations of PM_1, $PM_{2.5}$ and PM_{10} were 33.4 ± 15.4, 55.1 ± 27.3, 70.2 ± 34.1 μg m^{-3} during the YOG and increased by 48.2%, 32.9% and 39.6% after the YOG, respectively. The concentrations of NO_3^-, SO_4^{2-} and NH_4^+ remained at the same level before and during the YOG, but increased by 34.3%, 53.7%, 43.9% after the YOG, respectively. Also obvious increases of SO_2 by 84% and NO_2 by 32% were observed. The averaged concentrations of NO_2 were about 3-fold of SO_2 due to no restrictions on public travelling and strict control on the emission of SO_2 during the YOG. SOR varied from 0.15 to 0.82, with a mean of 0.52, NOR varied from 0.02 to 0.62 with a mean of 0.21, which led to relatively high ratio of SO_4^{2-}/NO_3^- by 1.4. Ca^{2+} increased about 2.2-fold, indicating elevated construction emissions in Nanjing after the YOG. There were no obvious diurnal variations of Ca^{2+} and SO_4^{2-} before and during the YOG, but high peak values of Ca^{2+} and SO_4^{2-} increased by 217%–366% and 138%–184% were observed in night hours owing to the rush of construction fields and heavy industry. Compared with concentration after the YOG, the averaged concentration of OC decreased by 8% and the EC concentration decreased by 28% during the YOG. The fraction of SOC of total carbon was 41% due to high potential photochemistry via regional transport during the YOG. The correlation coefficients between OC and EC were 0.82 during the YOG, and 0.61

after the YOG, which indicates that there are additional sources of OC after the control measures were canceled.

In summary, the air quality in Nanjing during the 2014 YOG improved a lot owing to the series of control measures implemented by the Nanjing municipal government and joint efforts in other YRD cities. Major control measures, e.g., the use of high quality coal and new electric buses, the closing of all construction facilities, the limiting of the production of some heavy industry, the forbiddance of high emission vehicles and outdoor barbecue restaurants, did take effect during the YOG. Regional joint emergency measures were added on while three events of deterioration of air quality occurred. However, the influence of secondary pollutants from regional scale, especially from the Shanghai-Nanjing city clusters, were clearly identified during the study period, suggesting that the government should consider long-term control strategy and establish collaborative control measures across administrative borders to achieve good air quality in the YRD.

ACKNOWLEDGMENTS

This study was supported by the National Science and Technology Support Program (2014BAC22B02), Air Pollution Control Technology Support Program of Jiangsu Province (BM2012063), Science and Technology Support Program of Jiangsu Province (SBE2014070928) and Jiangsu Natural Science Foundation (BK20131031 and BK20140021).

REFERENCES

Andersson, A., Deng, J., Du, K., Zheng, M., Yan, C., Skold, M. and Gustafsson, O. (2015). Regionally-varying combustion sources of the January 2013 severe haze events over eastern China. *Environ. Sci. Technol*. 49: 2038–2043.

Bauer, J.J., Yu, X., Cary, R., Laulainen, N. and Berkowitz, C. (2009). Characterization of the sunset semi-continuous carbon aerosol analyzer. *J. Air Waste Manage. Assoc.* 59: 826–833.

Cao, J.J., Lee, S.C., Chow, J.C., Watson, J.G., Ho, K.F., Zhang, R.J., Jin, Z.D., Shen, Z.X., Chen G.C., Kang, Y.M., Zou, S.C., Zhang, L.Z., Qi, S.H., Dai, M.H., Cheng, Y. and Hu, K. (2007). Spatial and seasonal distributions of carbonaceous aerosols over China. *J. Geophys. Res.* 112: D22S11.

Ding, A., Fu, C., Yang, X., Sun, J., Zheng, L., Xie, Y., Herrmann, E., Nie, W., Petaja, T., Kerminen, V. and Kulmala, M. (2013a). Ozone and fine particle in the western Yangtze River Delta: an overview of 1 yr data at the SORPES station. *Atmos. Chem. Phys.* 13: 5813–5830.

Ding, A.J., Fu, C.B., Yang, X.Q., Sun, J.N., Petaja, T., Kerminen, V.M., Wang, T., Xie, Y.N., Herrmann, E., Zheng, L.F., Nie, W., Wei, X.L. and Kulmala, M. (2013b). Intense atmospheric pollution modifies weather: A case of mixed biomass burning with fossil fuel combustion pollution in the eastern China. *Atmos. Chem. Phys*. 13: 10545–10554.

Ding, A., Wang, T. and Fu, C. (2013c). Transport characteristics and origins of carbon monoxide and ozone in Hong Kong, South China. *J. Geophys. Res.* 118: 9475–9488.

Ding, J., van der A.R.J., Mijling, B., Levelt, P.F. and Hao, N. (2015). NO_x emission estimates during the 2014 Youth Olympic Games in Nanjing. *Atmos. Chem. Phys.* 15: 9399–9412.

Ding, A.J., Nie, W., Huang, X., Chi, X., Sun, J., Kerminen, V.-M., Xu, Z., Guo, W., Petäjä, T., Yang, X., Kulmala, M. and Fu, C. (2016a). Long-term observation of air pollution-weather/climate interactions at the SORPES station: a review and outlook. *Front. Environ. Sci. Eng.* 10: 15.

Ding, A.J., Huang, X., Nie, W., Sun, J.N., Kerminen, V.M., Petaja, T., Su, H., Cheng, Y.F., Yang, X.Q., Wang, M.H., Chi, X.G., Wang, J.P., Virkkula, A., Guo, W.D., Yuan, J., Wang, S.Y., Zhang, R.J., Wu, Y.F., Song, Y., Zhu, T., Zilitinkevich, S., Kulmala, M. and Fu, C.B. (2016b). Enhanced haze pollution by black carbon in megacities in China. *Geophys. Res. Lett.* 43: 2873–2879.

Draxler, R.R. and Hess, G.D. (1998). An overview of the HYSPLIT_4 modelling system for trajectories. *Aust. Meteorol. Mag.* 47: 295–308.

Hao, N., Valks, P., Loyola, D., Cheng, Y.F. and Zimmer, W. (2011). Space-based measurements of air quality during the World Expo 2010 in Shanghai. *Environ. Res. Lett.* 6: 044004.

Huang, K., Zhuang, G., Lin, Y., Wang, Q., Fu, J.S., Fu, Q., Liu, T. and Deng, C. (2013). How to improve the air quality over megacities in China: pollution characterization and source analysis in Shanghai before, during, and after the 2010 World Expo. *Atmos. Chem. Phys.* 13: 5927–5942.

Huang, X., Song, Y., Li, M.M., Li, J.F., Huo, Q., Cai, X.H., Zhu, T., Hu, M. and Zhang, H.S. (2012). A high-resolution ammonia emission inventory in China. *Global Biogeochem. Cycles* 26: 239–256.

Huang, X., Song, Y., Zhao, C., Li, M.M., Zhu, T., Zhang, Q. and Zhang, X.Y. (2014). Pathways of sulfate enhancement by naturaland anthropogenic mineralaerosols in China. *J. Geophys. Res.* 119: 14165–14179.

Huang, X., Song, Y., Zhao, C., Cai, X., Zhang, H. and Zhu, T. (2015). Direct radiative effect by multicomponent aerosol over China. *J. Clim.* 28: 3472–3495.

Kong, L., Yang, Y., Zhang, S., Zhao, X., Du, H., Fu, H., Zhang, S., Cheng, T., Yang, X., Chen, J., Wu, D., Shen, J., Hong, S. and Jiao, L. (2014). Observations of linear dependence between sulfate and nitrate in atmospheric particles. *J. Geophys. Res.* 119: 341–361.

Li, B., Zhang, J., Zhao, Y., Yuan, S., Zhao, Q., Shen, G. and Wu, H. (2015). Seasonal variation of urban carbonaceous aerosols in a typical city Nanjing in Yangtze River Delta, China. *Atmos. Environ.* 106: 223–231.

Lin, Y., Huang, K., Zhuang, G., Fu, J. S., Xu, C., Shen, J. and Chen, S. (2013). Air quality over the Yangtze River Delta during the 2010 Shanghai Expo. *Aerosol Air Qual. Res.* 13: 1655–1666.

Liu, H., Wang, X., Zhang, J., He, K., Wu, Y. and Xu, J. (2013). Emission controls and changes in air quality in Guangzhou during the Asian Games. *Atmos. Environ.*

76: 81–93.

Mijling, B., van der A, R.J., Boersma, K.F., Van Roozendael, M., De Smedt, I. and Kelder, H.M. (2009). Reductions of NO_2 detected from space during the 2008 Beijing Olympic Games, *Geophys. Res. Lett.* 36: L13801.

Oxley, J.C., Kaushik, S.M. and Gilson, N.S. (1989). Thermal decomposition of ammonium nitrate-based composites. *Thermochim. Acta* 153: 269–286.

Pan, L., Tang, H. and Liu, X. (2015). Review and revelation of air quality assurance work during the Nanjing Youth Olympic Games. *Environ. Monit. Forewarning* 2015: 1–3 (in Chinese).

Shen, G., Xue, M., Yuan, S., Zhang, J., Zhao, Q., Li, B., Wu, H. and Ding, A. (2014). Chemical compositions and reconstructed light extinction coefficients of particulate matter in a mega-city in the western Yangtze River Delta, China. *Atmos. Environ.* 83: 14–20.

Stein, A.F., Draxler, R.R., Rolph, G.D., Stunder, B.J.B., Cohen, M.D. and Ngan, F. (2015). NOAA's HYSPLIT atmospheric transport and dispersion modeling system. *Bull. Am. Meteorol. Soc.* 96: 2059–2077.

Streets, D.G., Fu, J.S., Jang, C.J., Hao, J.M., He, K.B., Tang, X.Y., Zhang, Y.H., Wang, Z.F., Li, Z.P., Zhang, Q., Wang, L.T., Wang, B.Y. and Yu, C. (2007). Air quality during the 2008 Beijing Olympic Games. *Atmos. Environ.* 41: 480–492.

Tan, J., Duan, J., He, K., Ma, Y., Duan, F., Chen, Y. and Fu, J. (2009). Chemical characteristics of $PM_{2.5}$ during a typical haze episode in Guangzhou. *J. Environ. Sci.* 21: 774–781.

Tu, J., Xia, Z.G., Wang, H.S. and Li, W.Q. (2007). Temporal variations in surface ozone and its precursors and meteorological effects at an urban site in China. *Atmos. Res.* 85: 310–337.

Turpin, B.J. and Huntzicker, J.J. (1995). Identification of secondary organic aerosol episodes and quantitation of primary and secondary organic aerosol concentrations during SCAQS. *Atmos. Environ.* 29: 3527–3544.

Utsunomiya, A. and Wakamatsu, S. (1996). Temperature and humidity dependence on aerosol composition in the northern Kyushu, Japan. *Atmos. Environ.* 30: 2379–2386.

Wang, C., Zhang, X., Qin, W., Chen, W., Du, S. and Hu, Z. (2015). The research about air quality protection in the combined with observation for the Second Summer Youth Olympics Games. *Environ. Monit. Forewarning* 2015: 1–4 (in Chinese).

Wang, H.L., Qiao, L.P., Lou, S.R., Zhou, M., Ding, A.J., Huang, H.Y., Chen, J.M., Wang, Q., Tao, S.K., Chen, C.H., Li., L. and Huang, C. (2016). Chemical composition of $PM_{2.5}$ and meteorological impact among three years in urban Shanghai, China. *J. Cleaner Prod.* 112: 1302–1311.

Wang, T., Nie, W., Gao, J., Xue, L.K., Gao, X.M., Wang, X.F., Qiu, J., Poon, C.N., Meinardi, S., Blake, D., Wang, S.L., Ding, A.J., Chai, F.H., Zhang, Q.Z. and Wang, W.X. (2010). Air Quality during the 2008 Beijing Olympics: Secondary pollutants and regional impact. *Atmos. Chem. Phys.* 10: 7603–7615.

Wang, Z., Wang, T., Gao, R., Xue, L., Guo, J., Zhou, Y., Nie, W., Wang, X., Xu, P., Gao, J., Zhou, X., Wang, W. and Zhang, Q. (2011). Source and variation of carbonaceous aerosols at Mount Tai, North China: Results from a semi-continuous instrument. *Atmos. Environ.* 45: 1655–1667.

Wang, Z., Wang, T., Guo, J., Gao, R., Xue, L., Zhang, J., Zhou, Y., Zhou X., Zhang, Q. and Wang, W. (2012). Formation of secondary organic carbon and cloud impact on carbonaceous aerosols at Mout Tai, North China. *Atmos. Environ.* 46: 516–527.

Xie, Y.N., Ding, A.J., Nie, W., Mao, H.T., Qi, X.M., Huang, X., Xu, Z., Kerminen, V.M., Tuukka, P., Chi, X.G., Virkkula, A., Boy, M., Xue., L.K., Guo, J., Sun, J.N., Yang, X.Q., Kulamala, M. and Fu, C.B. (2015). Enhanced sulfate formation by nitrogen dioxide: Implications from in situ observations at the SORPES Station. *J. Geophys. Res.* 120: 12679–12694.

Xu, H.M., Tao, J., Ho, S.S.H., Ho, K.F., Cao, J.J., Li, N., Chow, J.C., Wang, G.H., Han, Y.M., Zhang, R.J., Watson, J.G. and Zhang, J.Q. (2013). Characteristics of fine particulate non-polar organic compounds in Guangzhou during the 16th Asian Games: Effectiveness of air pollution controls. *Atmos. Environ.* 76: 94–101.

Yuan, Z.B., Yu, J.Z., Lau, A.K.H., Louie, P.K.K. and Fung, J.C.H. (2006). Application of positive matrix factorization in estimating aerosol secondary organic carbon in Hong Kong and insights into the formation mechanisms, *Atmos. Chem. Phys.* 6: 25–34.

Zhang, X.Y., Wang, Y.Q., Lin, W.L., Zhang, Y.M., Zhang, X.C., Gong, S., Zhao, P., Yang, Y.Q., Wang, J.Z., Hou, Q., Zhang, X.L., Che, H.Z., Guo, J.P. and Li, Y. (2009). Changes of atmospheric composition and optical properties over Beijing 2008 Olympic Monitoring Campaign. *Bull. Am. Meteorol. Soc.* 90: 1633–1651.

Zhang, Y., Ding, A., Mao, H., Nie, W., Zhou, D., Liu ,L., Huang, X. and Fu, C. (2016). Impact of synoptic weather patterns and inter-decadal climate variability on air quality in the North China Plain during 1980-2013. *Atmos. Environ.* 124: 119–128.

Zhou, D.R., Ding, A.J., Mao, H.T., Fu, C.B., Wang, T., Chan, L.Y., Ding. K., Zhang. Y., Liu, J., Lu, A. and Hao, N. (2013). Impacts of the East Asian monsoon on lower tropospheric ozone over coastal South China. *Environ. Res. Lett.* 8: 044011.

Zhou, J., Zhang, R., Cao, J., Chow, J.C. and Watson, J.G. (2012). Carbonaceous and ionic components of atmospheric fine particles in Beijing and their impact on atmospheric visibility. *Aerosol Air Qual. Res.* 12: 492–502.

Received for review, May 13, 2016
Revised, October 19, 2016
Accepted, October 19, 2016